Research Article

Xiaochen Huang*, Yunfei Ding, Liang Li, Jinlong Ge, Yongkui Wang, Hao Zhao, Zijue Zhou and Hongyu Chen*

Influence of Ti_2SnC content on arc erosion resistance in Ag–Ti_2SnC composites

https://doi.org/10.1515/secm-2022-0244
received August 05, 2023; accepted February 16, 2024

Abstract: In this work, an Ag–Ti_2SnC composite was fabricated by the hot-pressing sintering method, and the erosion behavior of Ag–Ti_2SnC with volume percentages of 10–40% was studied at a load voltage of 10 kV. The arc life and breakdown current were observed at about 31–36 ms and 39 A, respectively. The cathode spot traveled the fastest on the surface of the Ag–40 vol% Ti_2SnC composite. Due to emission center model, the temperature of the minor protrusions on the cathode surface increased, resulting in Ag ions, Ti ions, and Sn ions being generated. Combining with the ionized oxygen, Ag_2O, AgO, TiO_2, and SnO_2 were formed on the eroded Ag–Ti_2SnC surface after arc erosion. The research results will broaden the application range of Ag–Ti_2SnC electrical contact material and enrich the arc erosion mechanism.

Keywords: contact material, cathode spot, Ag–Ti_2SnC composite, erosion behavior

1 Introduction

Satellite relays, rocket long-distance signal transmission, and circuit conversion essentially employ electrical contact materials. Arc erosion will degrade the material structure, reducing the service life of the material with considerable costs to the national economy. During arc combustion, the following features will be present: (1) The arc will travel on the material surface once it starts, where the higher the arc concentration and the harsher the erosion action on the material, the slower the motion speed. (2) The molten pool flow will accelerate through a combination of arc plasma force, static pressure, and other factors, resulting in splashing, pores, and bulges. The electrical contact material will repeat the molten pool creation, material splashing, material solidification, and pore formation processes after several arc erosion [1]. The electrical contact mechanical strength and conductivity of the material will be dramatically diminished, resulting in circuit breakdown, with a significant impact on signal transmission accuracy and efficacy. The microstructure of electrical contact materials will have an impact on arc combustion properties, and a good microstructure will accelerate arc movement and scatter the arc throughout the material surface. As a result, it is critical to choose the right electrical contact material.

By altering the preparation procedure, researchers have increased the arc erosion capabilities of materials. The contact materials prepared by internal oxidation exhibited fine and uniformly dispersed reinforcing phases, good reinforcing effect, excellent resistance to arc corrosion, and anti-melt welding [2–4]. However, oxygen diffusion was difficult to control, and the phenomenon of uneven oxidation was prone to occur. The improper selection of temperature during internal oxidation led to the inconsistency in oxide particle size and the decrease in electrical properties [5]. The powder metallurgy was commonly used in the fabrication of electrical contact materials. Compared with the internal oxidation and chemical coprecipitation methods [6], $AgSnO_2$ materials prepared by powder metallurgy showed less arc erosion and a shorter arc life [6,7]. The powders, such as Ag

* **Corresponding author: Xiaochen Huang**, School of Material and Chemical Engineering, Bengbu University, Anhui, 233030, China; Engineering Technology Research Center of Silicon-based Materials, Anhui, 233030, China, e-mail: xiaochenhuang@yeah.net
* **Corresponding author: Hongyu Chen**, College of Mechanical Engineering, Zhejiang University of Technology, Hangzhou, 310023, China, e-mail: 15222918166@163.com
Yunfei Ding: School of Mechanical and Ocean Engineering, Jiangsu Ocean University, Jiangsu, 222005, China
Liang Li, **Jinlong Ge**, **Yongkui Wang:** School of Material and Chemical Engineering, Bengbu University, Anhui, 233030, China; Engineering Technology Research Center of Silicon-based Materials, Anhui, 233030, China
Hao Zhao: School of Chemical and Materials Engineering, Anhui Science and Technology University, Bengbu, 233100, China
Zijue Zhou: School of Chemistry and Materials Engineering, Huainan Normal University, Huainan, 232001, China

and MAX/Ag and SnO_2/Ag, CuO, and In_2O_3, were first mixed by ball milling for some time, then the mixture was cold-pressed into the green bodies under a certain pressure. Thereafter, the green bodies were sintered for some hours at a certain temperature with flowing Ar [8–11]. Prior to sintering, the powder mixture was also annealed to release milling stress [12]. Ag and ZnO powders were first formed by cold isostatic press, and then the bulk materials were prepared by hot isostatic pressing [13]. In addition, due to the low sintering temperature and fast speed, Ag–WC, $AgSnO_2$, W–Cu–Ni electrical contact material via spark plasma sintering exhibited a high density and uniform structure [14–16]. AgZnO and Ag–Ti_3SiC_2 electrical contact material prepared by hot pressing sintering method also showed similar advantages [17,18]. Vacuum-assisted material extrusion was performed to eliminate matrix voids and improve the bonding quality of deposited layers by reducing heat loss and entrapped air during manufacturing [19–21]. The mechanical properties of the material obtained by vacuum-assisted material extrusion were improved compared with conventional methods, which may be introduced in the fabrication of electrical contact materials.

Adding additives and changing the distribution of additive CuO can greatly reduce the arc erosion of $AgSnO_2$ materials [12], which was another means to improve the material performance. Furthermore, adding Bi_2O_3, Y, or NiO was shown to improve the electrical contact properties of $AgSnO_2$ materials [4,22,23]. The physical properties of $AgSnO_2Bi_2O_3$ electrical contact materials can be improved through a combination of the melting atomization method and *in situ* reaction [24]. The addition of Ni was found to improve the arc erosion performance and dielectric strength of $AgTiB_2$ and CuCr materials, respectively [25]. After adding graphite to a CuW alloy, the arc was found to originally occur on the Cu-specific crystal orientation transferred to graphite, which greatly enhanced the arc erosion ability of the CuW alloy [26]. Carbon nanotubes have been shown to effectively promote arc dispersion in TiB_2/Cu materials and greatly reduce the arc energy of TiB_2/Cu materials [27]. Furthermore, an increase in W content can reduce the fusion welding force of Al_2O_3–Cu (Cr, w) materials and shorten the arc life [28]. However, additives can complicate the composition of electrical contact materials, making the preparation process difficult to control stably. Moreover, additives will increase the difficulty of material preparation and add to the production cost. Therefore, it is urgent to develop a new electrical contact material without additives.

MAX phase is a class of layered ternary compounds with unique metal and ceramic properties, where M corresponds to the early transition metal, A represents the A group element, and X represents carbon or nitrogen [29,30]. Compared with metals, MAX phase materials exhibit higher mechanical strength. The electrical and thermal conductivity of MAX phase are better than those of ceramics. In addition, the good mechanical processing performance of MAX phase materials is popular with researchers. Sun et al. claimed that the metal and MAX phase material did not diffuse or react at high temperatures without additives, proving that metal–MAX composites were suitable for electrical contact materials [8]. The typical representative of MAX is Ti_2SnC material. The electrical resistivity of Ti_2SnC material is 0.22 μΩ m. The temperature coefficient of resistivity is $0.0032\ K^{-1}$, and the coefficient of linear thermal expansion is $10 \times 10^{-6}\ K^{-1}$. The Young's modulus is 228 GPa and the Vickers hardness is 3.5 GPa [29]. Recently, Zhou et al. calculated the interface energy of Ag and Ti_2SnC using first principles based on density functional theory, it was expected to become a substitute for the new generation of electrical contact materials [31]. Therefore, it is feasible to choose Ti_2SnC as the reinforcing phase of Ag matrix as the electrical contact material [8,32–34]. Our previous work showed that Ti_3AlC_2/Ti_3SiC_2 material could protect the Cu/Ag matrix [18,35,36].

In this work, Ag–(10–40 vol%) Ti_2SnC composites were fabricated by the hot pressing sintering method, and the erosion behavior of the Ag–Ti_2SnC contact material in an air atmosphere was systematically studied.

2 Materials and methods

Ag powder (>99.9% purity, 200 mesh, Sinopharm Chemical Reagent Co., Ltd) and Ti_2SnC powder (>98%, 200 mesh, Laizhou Kai Kai Ceramic Materials Company Ltd) with different contents were first put into a sealed plastic bottle with a diameter of 80 mm and a height of 100 mm, and then the plastic bottle was placed and fixed inside a V-type mixing machine (VH5). The speed of the mixing machine containing the sealed plastic bottle was 120 rpm, maintaining for 2 h. The phases of the raw materials and the mixture were detected by X-ray diffraction (XRD, SmartLabSE, Japan) with Cu Ka radiation at 40 kV and 50 mA, as shown in Figure 2. The three-strong peaks ((111), (200), and (220)) of the Ag powder (JCPDF No. 87-0597) are labeled in Figure 2(a). The three strong peaks of the Ti_2SnC powder (JCPDF No. 29-1353) were located at the crystal planes of (002), (100), and (103), as indicated in Figure 2(b). The peak intensity of the Ti_2SnC of the mixture in Figure 2(c) increased with the increase in the Ti_2SnC content, which was much weaker than the Ag phase. These results were consistent with the ratio of raw materials. Then, the mixture was placed into a high-strength graphite

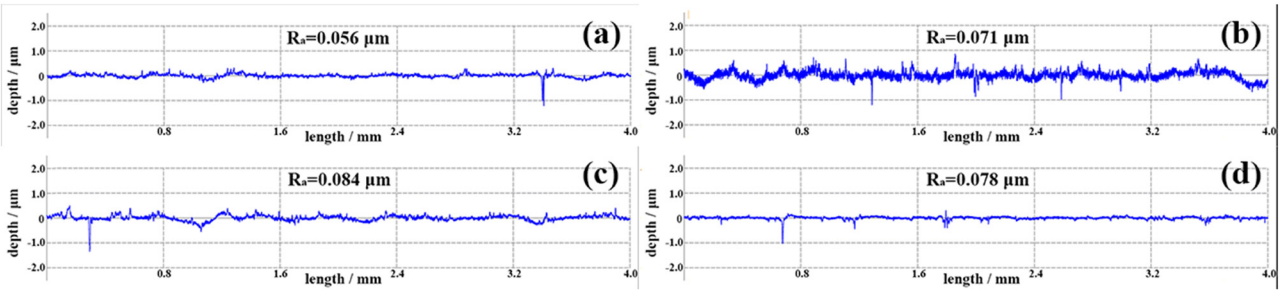

Figure 1: Curves of R_a vs length of (a) Ag–10 vol% Ti_2SnC, (b) Ag–20 vol% Ti_2SnC, (c) Ag–30 vol% Ti_2SnC, and (d) Ag–40 vol% Ti_2SnC.

mold and coated with BN on the inner wall. The mold was placed inside the hot-pressing sintering furnace (ZT-40-20Y, Shanghai Chenhua Science Technology Corp., Ltd), and 30 MPa of pressure was applied. After drawing air in the furnace to 10^{-5} Pa, argon gas was injected into the furnace. Subsequently, the mold was heated to 700°C and held for 30 min. Finally, for the phase detection and arc erosion test, the bulk was polished to a mirror surface using abrasive paper, and an optical microscope was employed to record the surface morphologies of the polished samples. The arithmetical mean deviation of profile (R_a) of polished Ag–Ti_2SnC samples, measured via Surface roughness tester (MarSurf PS 10) is displayed in Figure 1, where the value of R_a is less than 0.1 μm. The sintered density and relative density of Ag–Ti_2SnC composite, via Archimedes method are listed in Table 1. The arc erosion test was carried out using self-made arc erosion equipment. During the test, the polished sample and W rod were chosen as the cathode and anode, respectively, where a load voltage of 10 kV was applied to the electrodes. For details on the arc erosion progress, see the study by Huang et al. [37]. After the arc erosion test, a high-resolution oscilloscope (ADS1102CAL) was used to record the test parameters. Three-dimensional laser scanning confocal microscopy (3D LSCM, VK-X1000) was carried out to analyze and reconstruct the characteristics after the arc erosion test. To compare the composition changes of the sample, Raman spectroscopy (Lab RAM-HR) was used to determine the composition before and after arc erosion testing. The compositional changes and microstructures of the samples were recorded by a field-emission scanning electron microscope (FE-SEM, SU8020) equipped with energy dispersive spectroscopy (EDS).

Table 1: The sintered density and relative density of Ag–Ti_2SnC composite

Ti_2SnC content (vol%)	Sintered density (g/cm^3)	Relative density (%)
10	9.758	97.1
20	9.081	93.8
30	8.515	92.8
40	7.878	90.2

3 Results

3.1 Microstructure of fabricated samples

After sintering, the mixed powders turned to bulk, as shown in Figure 3(a1). As presented in Figure 3(a2), the sample had a mirror surface with a 15 mm diameter, and the height was about 3 mm. The XRD patterns of the samples (Ag–10–40 vol% Ti_2SnC) are shown in Figure 3(b). We observed that no other phase was detected on the surface, indicating that the silver powder did not react with the Ti_2SnC powder after sintering. From lines (5)–(8), the peak intensity of the Ti_2SnC phase increased with the increase in the Ti_2SnC content. The Raman spectroscopy results of the polished sample are shown in Figure 3(c), and the laser acted inside the yellow rectangle in the inset. The 247 cm^{-1} peak was labeled in the spectrum, which belonged to Ti_2SnC [38], indicating that the gray phase was Ti_2SnC. The optical micrographs of the Ag–Ti_2SnC composite are displayed in Figure 4. The gray phases were evenly distributed on the surface, and we observed that with an increase in Ti_2SnC content, the gray phase increased gradually.

3.2 Arc parameters of eroded Ag–Ti_2SnC cathodes

The current–time curves of the Ag–Ti_2SnC composite are shown in Figure 5, where the vertical axis indicates the current value in the figure. Once an arc occurs, the current reaches the maximum first and is called the breakdown

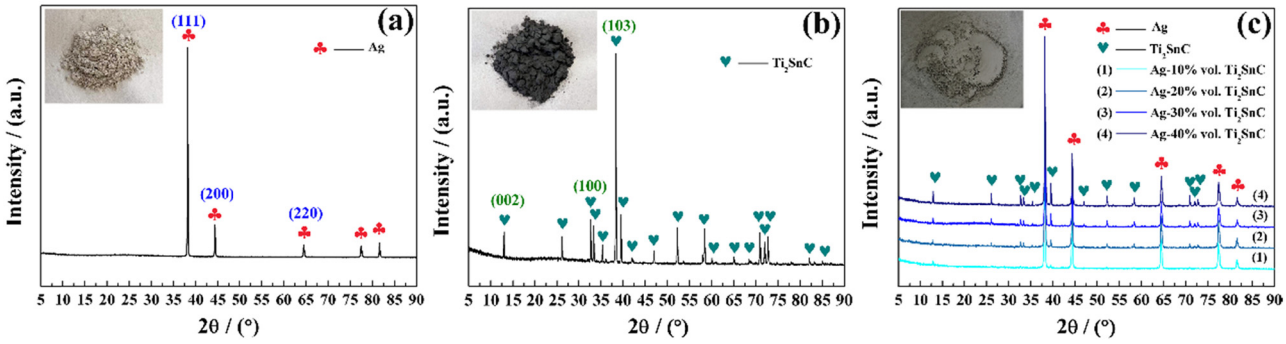

Figure 2: XRD patterns of (a) the Ag powder, (b) Ti_2SnC powder, and (c) mixture of Ag with 10–40 vol% Ti_2SnC powder.

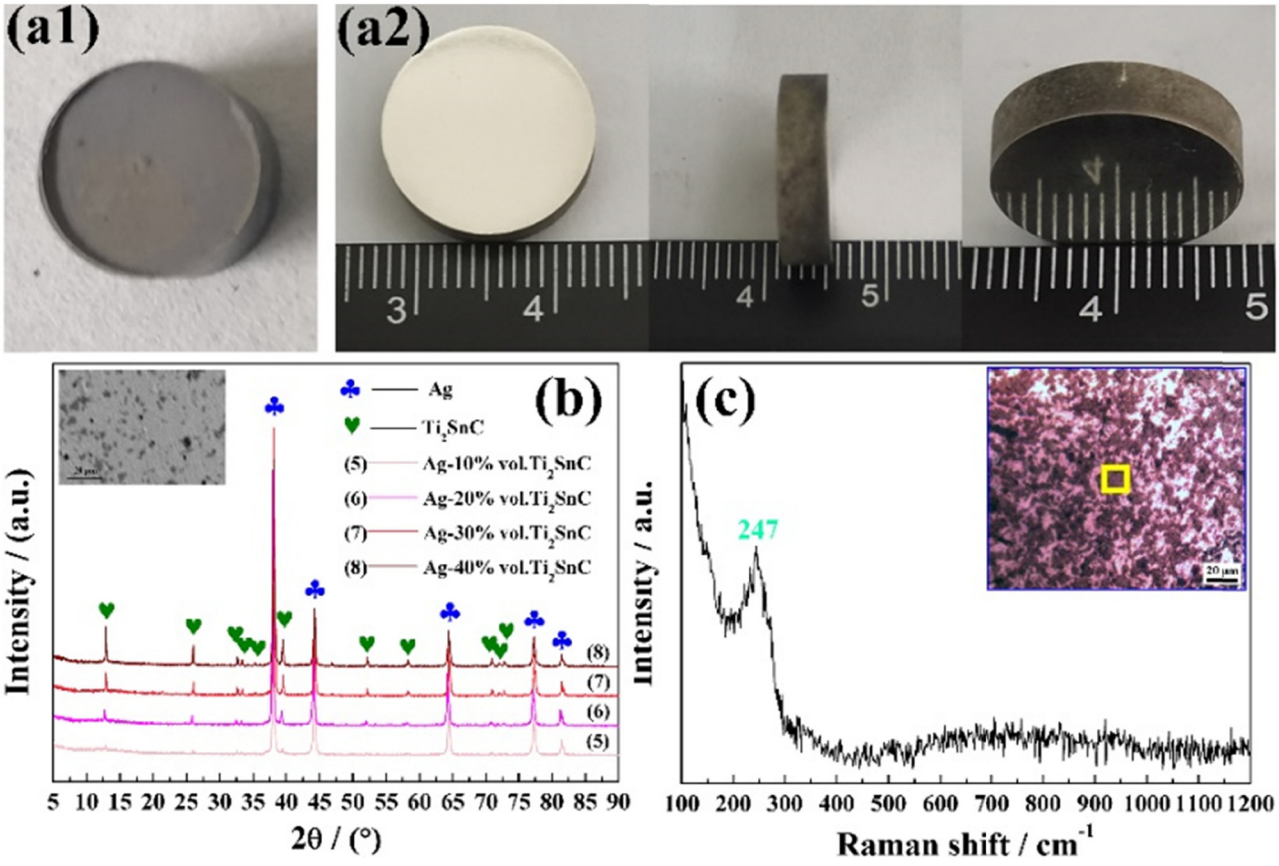

Figure 3: (a1) The sintered block; (a2) the polished samples; (b) XRD pattern of the Ag–(10–40 vol%) Ti_2SnC composite; and (c) Raman spectroscopy of the Ag–40 vol% Ti_2SnC composite.

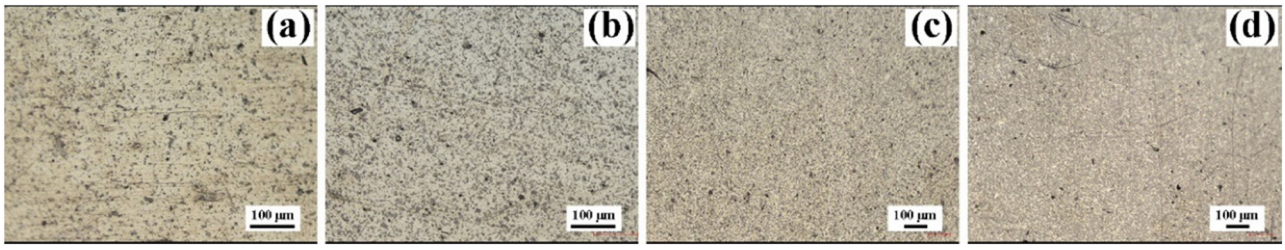

Figure 4: Optical micrographs of (a) Ag–10 vol% Ti_2SnC; (b) Ag–20 vol% Ti_2SnC; (c) Ag–30 vol% Ti_2SnC; and (d) Ag–40 vol% Ti_2SnC composite.

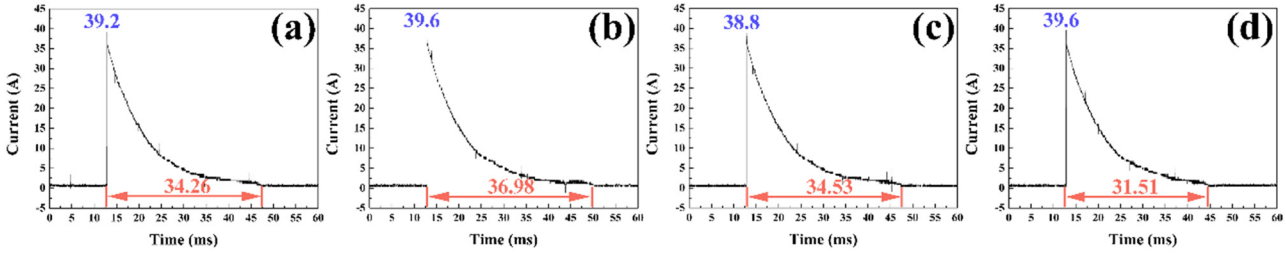

Figure 5: Current–time curves at a load voltage of 10 kV for the Ag–Ti_2SnC composite with Ti_2SnC of (a) 10 vol%, (b) 20 vol%, (c) 30 vol%, and (d) 40 vol%.

current. The breakdown current of the Ag–Ti_2SnC composite was around 39 A with Ti_2SnC content from 10 to 40 vol%. When the current value was close to zero, the arc was extinguished. The period from the beginning of arc erosion to extinction is called arc life. The values of arc life and breakdown current are displayed in Table 2. The arc life of the Ag–Ti_2SnC composite remained about 31–36 ms. The arc energy was related to the arc life, breakdown current, and load voltage, which can be calculated using equation (1) [39].

$$E = U I t, \tag{1}$$

where E is the arc energy (J), U is the load voltage (kV), I is the breakdown current (A), and t is the arc life (ms). The calculation results are listed in Table 2. The breakdown current of Ag–40 vol% Ti_2SnC was 39.6 A, which was much lower than Ag–40 vol% Ti_3SiC_2 (50.2 A) [18]. Similarly, the arc energy of the Ag–Ti_2SnC composite was about 12–14 kJ, which was also lower than Ag–Ti_3SiC_2 at the same load voltage [18]. The electric current of AgZnO [13], $AgSnO_2$ [11], AgCuO [40], $AgCuOIn_2O_3SnO_2$ [10], AgWC30 [41], $AgTiB_2$ [25], $AgTiB_2WO_3$ [42], Al_2O_3-Cu/(W, Cr) [28], and Ag–$La_2Sn_2O_7$/SnO_2 [43] ranged from 10 to 30 A. The arc voltage of those electrical contact materials varied from 12 to 4,500 V. The arc current and voltages used in the above materials were small, the arc energy was therefore far less than that of Ag–Ti_2SnC material (12478 J-14644 J). However, due to the smaller arc energy for one arc erosion, the experiment was needed to be carried out tens of thousands of times [10,11,13,25,40–49]. That is why only one time arc erosion experiment was carried out here, where a single arc energy was sufficient to damage the surface of Ag–Ti_2SnC electric contact material, and the surface morphology and composition could be analyzed.

Table 2: Arc parameters of the Ag–Ti_2SnC composite at a load voltage of 10 kV

Ti_2SnC content (vol%)	10	20	30	40
Breakdown current (A)	39.2	39.6	38.8	39.6
Arc life (ms)	34.26	36.98	34.53	31.51
Arc energy ($\times 10^3$ J)	13.430	14.644	13.398	12.478

3.3 Morphology and content on the eroded surface

To observe the morphological characteristics after arc erosion, 3D LSCM was used to record the overall morphology and three-dimensional characteristics. The image shown in Figure 6 was obtained by the laser and color mode, and the eroded center areas are labeled by circles in the figure. With an increase in Ti_2SnC content from 10–30 vol%, the erosion center area gradually became larger. As shown in Figure 6(a)–(c), the arc was concentrated at one point, forming a circle arc area on the surface. When the Ti_2SnC content increased to 40 vol%, an interesting phenomenon occurred, and the arc area was no longer concentrated at one point. After the arc started at one point, as shown by the circle in Figure 6(d), it jumped on the Ag–40 vol% Ti_2SnC composite surface very fast. The arc life of the Ag–40 vol% Ti_2SnC composite was 31.51 ms, which was the shortest among the Ag–Ti_2SnC composite. This phenomenon was consistent with the movement of the cathode spot, which will be further discussed in Section 4.3. The three-dimensional morphology is shown in Figure 7, and except for Figure 7(c), the morphology of the Ag–Ti_2SnC composite after arc erosion was even without obvious bulges and pores. The arc concentrated at one point on the Ag–30 vol% Ti_2SnC composite surface, causing the arc energy to concentrate at this point. When the arc was extinguished, numerous bulges and pores formed on the surface.

To determine the chemical composition change of the eroded Ag–Ti_2SnC composite, the microstructure was further amplified by a SEM, as shown in Figure 8, where the morphologies in Figure 8(b) and (c) corresponded to the morphologies inside the same color rectangle in Figure 8(a). Many bulges formed on the eroded Ag–Ti_2SnC composite surface, as

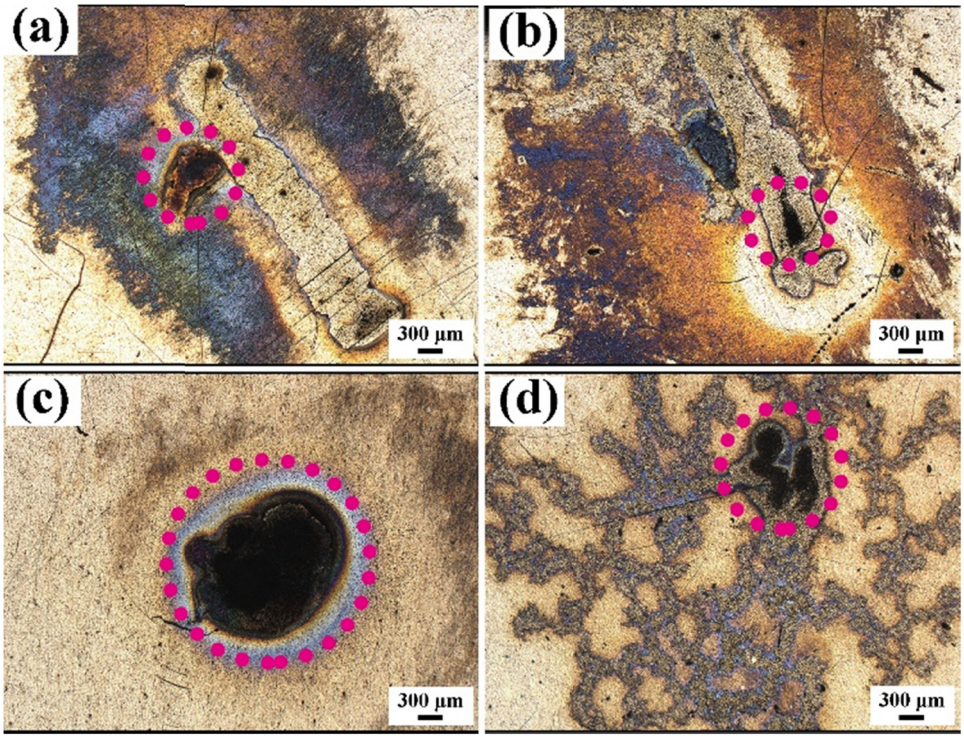

Figure 6: Micro-images of the eroded Ag–Ti_2SnC with Ti_2SnC content values of (a) 10 vol%, (b) 20 vol%, (c) 30 vol%, and (d) 40 vol% obtained in laser color mode using a three-dimensional laser scanning confocal microscope.

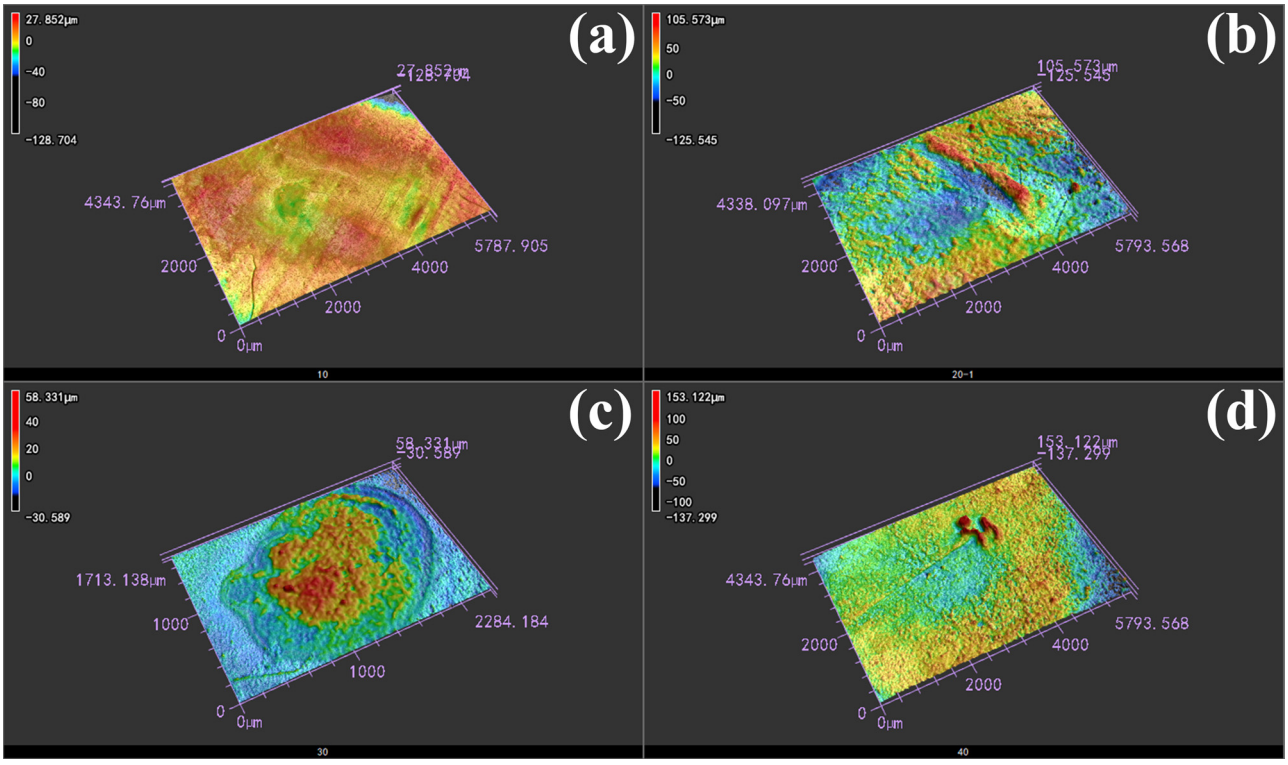

Figure 7: Three-dimensional morphology of eroded Ag–Ti_2SnC with the Ti_2SnC content of (a) 10 vol%, (b) 20 vol%, (c) 30 vol%, and (d) 40 vol%.

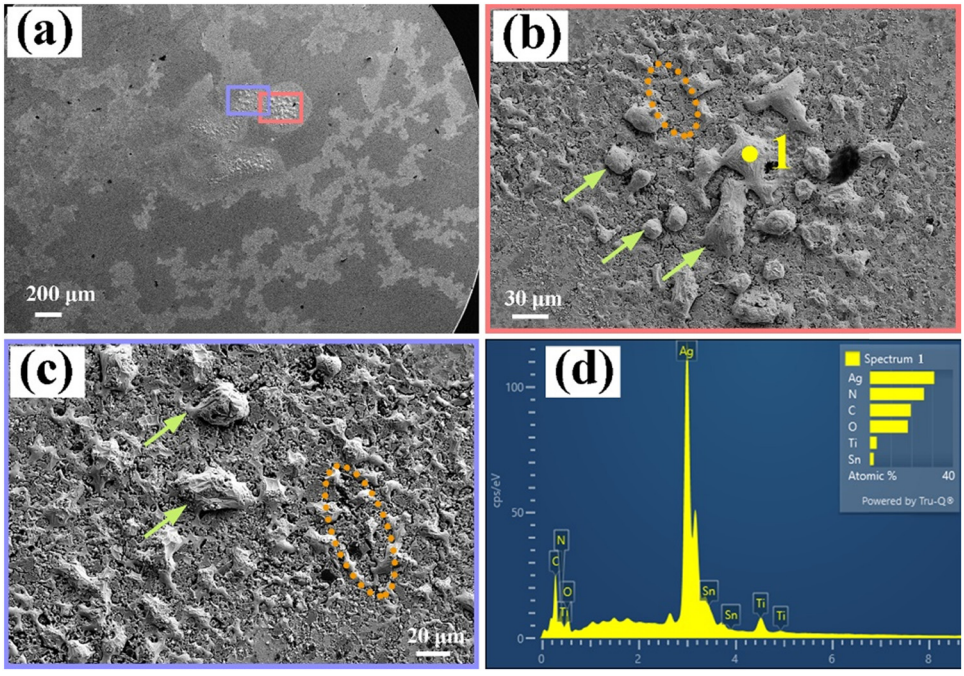

Figure 8: (a) SEM of Ag–40 vol% Ti_2SnC; (b) and (c) amplified images of (a); (d) the EDS result of point 1 in (b).

indicated by the arrows in Figure 8(b) and (c), and microcracks are indicated by the circles in Figure 8(b) and (c). Spot scanning acted at point 1 in Figure 8(b), and the results are shown in Figure 8(d). After arc erosion, Ag, Ti, and Sn elements were detected on the eroded surface. Furthermore, N and O elements were found in the EDS results, indicating that oxides or nitrides were generated after the arc erosion test.

To further clarify the products after arc erosion, Raman spectroscopy was carried out on the eroded area. The results are presented in Figure 9, where the laser acted on the areas in the yellow rectangles inside the insets. At the edge of the erosion area in Figure 9(a), the peaks (247, 669, and 916 cm^{-1}) of Ti_2SnC were observed [38,50]. The peak at 1,049 cm^{-1} in the Raman shift belonged to the Ag element (R0070754), and the peak value of 1,121 cm^{-1} belonged to SnO_2 (R040072). The results in Figure 9(a) indicated that a part of Ti_2SnC decomposed and was oxidized at the eroded area. When the laser acted at the yellow rectangle in Figure 9(b), the peaks of 885 and 1,054 cm^{-1} were detected, which belonged to Ag_2O [51]. Except for Ag_2O (935 and 1,059 cm^{-1}) [51,52], the peaks belonging to AgO (302 and 990 cm^{-1}) [53,54] and SnO_2 (691 and 818 cm^{-1}, R050502 and R040017) were found in the Raman shift in Figure 9(c). As shown in Figure 9(d), the peaks at 148, 202, and 516 cm^{-1} were attributed to TiO_2 (R050363, R120013, and R070582), and the peak at 247 cm^{-1} was assigned to Ti_2SnC [38]. The four characteristic bands at 335, 781, 870, and 967 cm^{-1} were assigned to SnO_2 (R050502, R040017, R050502, and R060563), and the 1,072 cm^{-1} peak belonged to Ag_2O [52]. The Raman spectra in Figure 9 indicated that the Ag–Ti_2SnC composite decomposed and oxidized to AgO, Ag_2O, TiO_2, and SnO_2. No nitrides were detected on the eroded surface.

4 Discussion

4.1 Generation of arc discharge

Gas discharge can be divided into non-self-sustained discharge and self-sustained discharge. When the current between the two electrodes was greater than a certain value, the gas conduction process itself could produce the charged particles needed to maintain conduction. This type of gas discharge only required additional measures to produce charged particles and induce ignition at the beginning. Once the discharge started, the additional measures were canceled, and the discharge process could continue. The discharge process itself could produce the charged particles required to maintain the discharge, which was called self-sustaining discharge [55]. The arc discharge belonged to the self-sustaining discharge and the arc discharge possessed the characteristics of lowest voltage, maximum current, highest temperature, and strongest luminescence. The charged particles that could maintain

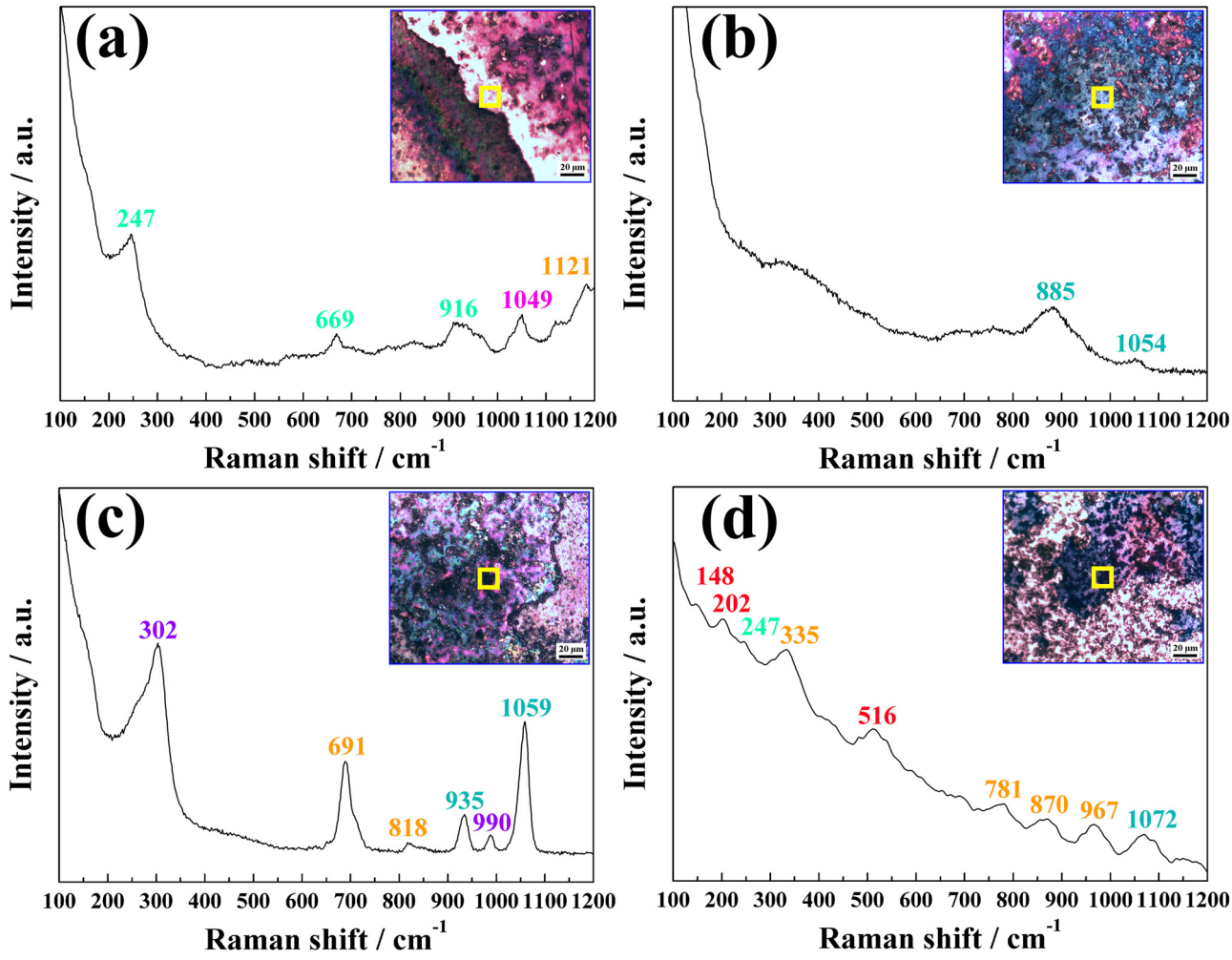

Figure 9: Raman spectra of the eroded Ag–Ti_2SnC composite of (a) Ti_2SnC and SnO_2, (b) Ag_2O, (c) AgO, Ag_2O and SnO_2, (d) TiO_2, Ti_2SnC, SnO_2 and Ag_2O.

arc combustion consisted of electrons, positive ions, and negative ions. These particles were mainly produced by two physical processes, namely, gas ionization between the electrodes and electron emissions on the electrode surface. At the same time, this was accompanied by other processes such as dissociation, excitation, and recombination.

Although Ag–Ti_2SnC composites were polished to a mirror face, the surface roughness of Ag–Ti_2SnC is shown in Figure 1. It can be seen that the value of R_a was less than 0.1 μm, meaning that there were still some minor protrusions existing on the cathode surface. According to the emission center model, the field strength at the micro protrusions on the cathode surface are very strong, and the heat generated by the field electron emission current in the area will increase the temperature at the micro protrusions. If the temperature is increased to a certain height, the field emissions will change into blasting electron emissions [56]. The minor protrusions existed on the cathode surface. When a load voltage of 10 kV was applied to the electrodes, the temperature of the minor protrusions increased. If the energy were to exceed the work function of the surface electrons, the electrons would escape from the surface. After electrons escaped, the Ag–Ti_2SnC cathodes with lost electrons would become Ag ions, Ti ions, and Sn ions. The escaped electrons and these positive ions together formed a metal vapor. In 1971, Boddy and Utsumi first discovered that under atmospheric pressure, the arc combustion process was divided into two stages, namely, metallic phase and gaseous phase [57]. Thereafter, two main phases (metallic phase and gaseous phase) were proven to be present in the break arcs of resistive circuits spectroscopically [58]. In addition, the second gaseous phase is not present in vacuum arcs [58]. Since metal ions are eliminated in the process of inter-diffusion, the gas phase arc generated by ionization of the surrounding gas particles plays a greater part. The electrons on the cathode surface could also be emitted by light, an electric field, and particle collision [59].

Furthermore, the charged particles that sustained arc combustion were also ionized by gas. Under the action of an electric field between the two electrodes, the electrons moved toward the anode. During this process, the electrons collided with the atoms in the air, causing atoms to ionize into positive and negative ions, which was known as gaseous phase. In addition, the gas particles could be ionized by heat and light. The transition boundary from metallic to gaseous phase was closely related to arc voltage, air pressure, gas types, materials, and so on [60–62]. Kiyoshi Yoshida and Sunao Tanimoto experimentally studied the arc transition from metallic to gaseous phase in Ag, AgCu, and $AgSnO_2$ [63,64]. The experiment was executed within the range of the source voltage from 12 to 48 V in air condition. They concluded that the gaseous phase arc transit was not caused in 24 V or less [65]. Here the arc voltage was 10 kV, which was much more than 24 V. In addition, arc erosion test was carried out under air condition. Therefore, the arc combustion process of Ag–Ti_2SnC, specifically the plasma cloud, was formed by the combination of metal vapor and gas ionization. Considering the complexity of factors affecting arc transition from metallic to gaseous phase, it is necessary to further study the arc transition of Ag–Ti_2SnC under air condition.

4.2 Movement of the cathode spot

During arc combustion, we observed a very bright plasma region with irregular movement on the cathode surface, which was called the cathode spots. These cathode spots were the center of emitting electrons, ions, metal vapor, and ejected droplets, which played a decisive role in the erosion of electrode materials and the continuity of current [56]. If a micro protrusion was completely consumed, the cathode spot would appear at the nearest neighboring protrusions until the arc was extinguished. When the content of Ti_2SnC increased, the boundaries between Ag and Ti_2SnC increased, resulting in the formation of more protrusions during the polishing process. Although the arc life was about 31–36 ms, the increase in protrusions on the surface of Ag–40 vol% Ti_2SnC could cause the cathode spots to move to a longer distance than Ag–30 vol% Ti_2SnC. In the cathode spot area, molten pools formed, causing the Ag–Ti_2SnC cathodes to melt and splash. Under the action of the Marangoni effect, bulge morphologies formed in Figure 8(b) and (c) [66]. When the arc was extinguished, the molten material solidified, and minor cracks and bulges formed on the surface.

4.3 Phase change after arc erosion

During arc combustion, Ag and Ti_2SnC on the cathode surface decomposed into Ag ions, Ti ions, and Sn ions, and these ions combined with the O anions ionized in the air to form TiO_2, SnO_2, AgO, and Ag_2O, as shown in Figures 8(d) and 9. Due to good wettability between Ag and SnO_2 [32], SnO_2 was likely the new starting point for cathode spot movement. Therefore, the movement range of the cathode spots on the material surface was the largest on the surface of Ag–40 vol% Ti_2SnC, resulting in the morphology shown in Figure 6(d).

5 Conclusion

Ag–Ti_2SnC composite was fabricated by the hot-pressing sintering method. The erosion behavior of the Ag–Ti_2SnC composite with varying contents of Ti_2SnC was studied.

1) The breakdown current of Ag–Ti_2SnC composite is around 39 A with the Ti_2SnC content varying from 10 to 40 vol%, which is lower than that of Ti_3SiC_2 (52.6 A) material in our previous study. The arc energy of Ag–Ti_2SnC composite is about 12–14 kJ, which is also lower than that of Ag–Ti_3SiC_2 at the same load voltage.
2) The arc concentrates at one point on Ag–(10–30)vol% Ti_2SnC composite surface. The arc jumps on the Ag–40 vol% Ti_2SnC composite surface very fast. The arc life of Ag–40 vol% Ti_2SnC composite is 31.51 ms, which is the shortest among the Ag–Ti_2SnC composite.
3) The morphologies of bulges and pores are formed on the eroded surface of the Ag–Ti_2SnC composite.
4) Metal oxides, such as Ag_2O, AgO, TiO_2, and SnO_2 are detected on the surface.
5) During arc combustion, Ag and Ti_2SnC on the cathode surface decomposed into Ag ions, Ti ions, and Sn ions. The arc combustion process of Ag–Ti_2SnC was formed by the combination of metal vapor and gas ionization, which may be measured by spectrometric method systematically in the future.

Acknowledgements: This work was supported by the Natural Science Foundation of Anhui Province (Grant Nos 2208085ME104 and 1908085QE218), the University Natural Science Research Project of Anhui Province (Grants Nos KJ2021ZD0141 and 2022AH051589), the National Science Foundation of China

(Grant Nos 52275467, 51905485, and 51971100), Cultivation Programme for the Outstanding Young Teachers of Anhui Province (YQYB2023054) and Anhui Province Key Laboratory of Coal Clean Conversion and High Valued Utilization, Anhui University of Technology (CHV19-05).

Funding information: This work was financially supported by the Natural Science Foundation of Anhui Province (Grant Nos 2208085ME104 and 1908085QE218), the University Natural Science Research Project of Anhui Province (Grants Nos KJ2021ZD0141 and 2022AH051589), the National Science Foundation of China (Grant Nos 52275467, 51905485, and 51971100), Cultivation Programme for the Outstanding Young Teachers of Anhui Province (YQYB2023054) and Anhui Province Key Laboratory of Coal Clean Conversion and High Valued Utilization, Anhui University of Technology (CHV19-05).

Conflict of interest: The authors state no conflict of interest.

Data availability statement: The datasets generated during and/or analyzed during the current study are available from the corresponding author on reasonable request.

References

[1] Ding KK, Ding JX, Zhang KG, Chen LM, Ma CJ, Bai ZC, et al. Micro/nano-mechanical properties evolution and degradation mechanism of Ti_3AlC_2 ceramic reinforced Ag-based composites under high-temperature arc corrosion. Ceram Int. 2022;48(22):33670–81.

[2] Xu CH, Yi DQ, Wu CP, Liu HQ, Li WZ. Microstructures and properties of silver-based contact material fabricated by hot extrusion of internal oxidized Ag–Sn–Sb alloy powders. Mater Sci Eng A. 2012;538:202–9.

[3] Lutz O, Behrens V, Franz S, Honig T, Heinrich J, Aichele I, et al. Silver/tin oxide contact materials based on internal oxidation for AC and DC applications. VDE Fachberichte. 2009;167–76.

[4] Zhou XL, Xiong AH, Liu MM, Zheng Z, Yu J, Wang LH. Electrical contact properties of $AgSnO_2NiO$ electrical contact material. Rare Met Mater Eng. 2019;48(9):2885–92.

[5] Pedder DJ. The thermal stability of cadmium oxide in internally oxidized silver-cadmium alloys. Metall Trans A. 1978;9(5):659–70.

[6] Wu CP, Zhao Q, Li NN, Wang HS, Yi DQ, Weng W. Influence of fabrication technology on arc erosion of $Ag/10SnO_2$ electrical contact materials. J Alloy Compd. 2018;766:161–77.

[7] Chen HY, Xu Q, Wang JH, Li P, Yuan JL, Lyu BH, et al. Effect of surface quality on hydrogen/helium irradiation behavior in tungsten. Nucl Eng Technol. 2022;54(6):1947–53.

[8] Ding JX, Tian WB, Wang DD, Zhang PG, Chen J, Zhang YM, et al. Corrosion and degradation mechanism of Ag/Ti_3AlC_2 composites under dynamic electric arc discharge. Corros Sci. 2019;156:147–60.

[9] Ding JX, Tian WB, Zhang PG, Zhang M, Zhang YM, Sun ZM. Arc erosion behavior of Ag/Ti_3AlC_2 electrical contact materials. J Alloy Compd. 2018;740:669–76.

[10] Hu C, Zhou XL, Chen L, Liu MM, Wang LH. Effect of SnO_2 additive on the electrical contact properties of $AgCuOIn_2O_3$ composites. Acta Materiae Compositae Sin. 2022;39(3):1322–31.

[11] Zhang M, Wang XH, Yang XH, Zou JT, Liang SH. Arc erosion behaviors of $AgSnO_2$ contact materials prepared with different SnO_2 particle sizes. Trans Nonferrous Met Soc China. 2016;26:783–90.

[12] Wang J, Kang YQ, Wang C, Wang JB, Fu C. Resistance to arc erosion characteristics of CuO skeleton-reinforced Ag-CuO contact materials. J Alloy Compd. 2018;756:202–7.

[13] Li AK, Nie BX, Xie M, Wang S, Chen Y, Zhu YF, et al. Microstructure and property research on AgZnO electrical contact materials prepared by hot isostatic pressing Precious. Metals. 2018;39(51):14–20.

[14] Ray N, Kempf B, Wiehl G, Mützel T, Heringhaus F, Froyen L, et al. Novel processing of Ag-WC electrical contact materials using spark plasma sintering. Mater Des. 2017;121:262–71.

[15] Xiong QF, Wang S, Xie M, Chen YT, Zhang JM, Wang SB. $AgSnO_2$ electrical contact material prepared by spark plasma sintering. Precious Met. 2013;34(4):12–6.

[16] Lungu M, Tsakiris V, Enescu E, Pătroi D, Marinescu V, Tălpeanu D, et al. Development of W-Cu-Ni electrical contact materials with enhanced mechanical properties by spark plasma sintering process. Acta Phys Polonica A. 2014;125:327–30.

[17] Guzmán D, Muñoz P, Aguilar C, Iturriza I, Lozada L, Rojas PA, et al. Synthesis of Ag–ZnO powders by means of a mechanochemical process. Appl Phys A. 2014;117(2):871–5.

[18] Huang XC, Feng Y, Ge JL, Li L, Li ZQ, Ding M. Arc erosion mechanism of $Ag\text{-}Ti_3SiC_2$ material. J Alloy Compd. 2020;817:152741.

[19] Cao D. Investigation into surface-coated continuous flax fiber-reinforced natural sandwich composites via vacuum-assisted material extrusion. Prog Addit Manuf. 2023. doi: 10.1007/s40964-023-00508-6

[20] Cao D. Fusion joining of thermoplastic composites with a carbon fabric heating element modified by multiwalled carbon nanotube sheets. Int J Adv Manuf Technol. 2023;128(9):4443–53.

[21] Cao D, Bouzolin D, Lu H, Griffith DT. Bending and shear improvements in 3D-printed core sandwich composites through modification of resin uptake in the skin/core interphase region. Compos Part B: Eng. 2023;264:110912.

[22] Wang HT, Wang LZ, Wang ZX. Physical and electrical contact properties of $Ag\text{-}SnO_2$ contact materials doped with different particle size additives. Rare Met Mater Eng. 2019;48(2):458–62.

[23] Wang JQ, Zhang Y, Kang HL. Study on properties of $AgSnO_2$ contact materials doped with rare earth Y. Mater Res Express. 2018;5(8):085902.

[24] Wu XH, Yang H, Qi GX, Zhang LJ, Shen T, Mu CF, et al. A study on preparation and properties of $Ag/SnO_2\text{-}Bi_2O_3$ electrical contact materials via in-situ reaction method. Electr Mater. 2019;5:6–11.

[25] Li HY, Wang XH, Xi Y, Zhu T, Guo XH. Effect of Ni addition on the arc erosion behavior of $AgTiB_2$ contact material. Vacuum. 2019;161:361–70.

[26] Chen QY, Liang SH, Wang F, Zhuo LC. Microstructural investigation after vacuum electrical breakdown of the W-30wt.%Cu contact material. Vacuum. 2018;149:256–61.

[27] Long F, Guo XH, Song KX, Jia SG, Yakubov V, Li SL, et al. Enhanced arc erosion resistance of TiB_2/Cu composites reinforced with the carbon nanotube network structure. Mater Des. 2019;183:108136.

[28] Zhang XH, Zhang Y, Tian BH, An JC, Zhao Z, Volinsky AA, et al. Arc erosion behavior of the Al_2O_3-Cu/(W, Cr) electrical contacts. Compos Part B: Eng. 2019;160:110–8.

[29] Sun ZM. Progress in research and development on MAX phases: a family of layered ternary compounds. Int Mater Rev. 2011;56(3):143–66.
[30] Barsoum MW. The $M_{N+1}AX_N$ phases: A new class of solids: Thermodynamically stable nanolaminates. Prog Solid State Chem. 2000;28(1):201–81.
[31] Nian Y, Zhang Z, Liu M, Zhou X. The electronic structure and stability of Ti_2SnC/Ag interface studied by first-principles calculations. Adv Theory Simul. 2023;7:2300649.
[32] Ding JX, Tian WB, Zhang PG, Zhang M, Chen J, Zhang YM, et al. Preparation and arc erosion properties of Ag/Ti_2SnC composites under electric arc discharging. J Adv Ceram. 2019;8(1):90–101.
[33] Zhang M, Tian WB, Zhang PG, Ding JX, Zhang YM, Sun ZM. Microstructure and properties of Ag–Ti_3SiC_2 contact materials prepared by pressureless sintering. Int J Miner Metall Mater. 2018;25(7):810–6.
[34] Ding JX, Sun ZM, Zhang PG, Tian WB, Zhang YM. Current research status and outlook of Ag-based contact materials. Materials Reports. 2018;32(1):58–66.
[35] Huang XC, Feng Y, Qian G, Ge JL, Zhang XF, Wang CH. Comparison of electrical ablation properties between pantograph materials: Ti_3AlC_2 and Cu-Ti_3AlC_2. Rare Met Mater Eng. 2020;49(1):34–41.
[36] Huang XC, Feng Y, Qian G, Zhao H, Song ZK, Zhang JC, et al. Arc corrosion behavior of Cu-Ti_3AlC_2 composites in air atmosphere. Sci China Technol Sci. 2018;61(4):551–7.
[37] Huang XC, Feng Y, Qian G, Zhou ZJ. Arc ablation properties of Ti_3SiC_2 material. Ceram Int. 2019;45(16):20297–306.
[38] Bentzel GW, Naguib M, Lane NJ, Vogel SC, Presser V, Dubois S, et al. High-temperature neutron diffraction, Raman spectroscopy, and first-Principles calculations of Ti_3SnC_2 and Ti_2SnC. J Am Ceram Soc. 2016;99(7):2233–42.
[39] Kubo S, Kato K. Effect of arc discharge on the wear rate and wear mode transition of a copper-impregnated metallized carbon contact strip sliding against a copper disk. Tribol Int. 1999;32:367–78.
[40] Chen SY, Wang J, Yuan Z, Wang Z, Du D. Microstructure and arc erosion behaviors of Ag-CuO contact material prepared by selective laser melting. J Alloy Compd. 2021;860:158494.
[41] Ren XL, Chen S, Li MY, Xie M, Chen JH, Wang SB, et al. Arc erosion characteristics of AgWC30 electrical contact material. Rare Met Mater Eng. 2017;46(11):3345–51.
[42] Li HY, Wang XH, Xi Y, Liu YF, Guo XH. Influence of WO_3 addition on the material transfer behavior of the $AgTiB_2$ contact material. Mater & Des. 2017;121:85–91.
[43] Zhang LJ, Shen T, Shen QH, Zhang J, Chen L, Fan XP, et al. Anti-arc erosion properties of Ag-$La_2Sn_2O_7$/SnO_2 contacts. Rare Met Mater Eng. 2016;45(7):1664–8.
[44] Wang XH, Yang H, Chen M, Zou JT, Liang SH. Fabrication and arc erosion behaviors of $AgTiB_2$ contact materials. Powder Technol. 2014;256:20–4.
[45] Wang XH, Yang H, Liang SH, Liu MB, Liu QD. Effect of TiB_2 particle size on erosion behavior of Ag-4wt% TiB_2 composite. Rare Met Mater Eng. 2015;44(11):2612–7.
[46] Li HY, Wang XH, Liu YF, Guo XH. Effect of strengthening phase on material transfer behavior of Ag-based contact materials under different voltages. Vacuum. 2017;135:55–65.
[47] Li HY, Wang XH, Guo XH, Yang XH, Liang SH. Material transfer behavior of $AgTiB_2$ and $AgSnO_2$ electrical contact materials under different currents. Mater Des. 2017;114:139–48.
[48] Ding JX, Tian WB, Wang DD, Zhang PG, Chen J, Sun ZM. Arc erosion and degradation mechanism of Ag/Ti_2AlC composite. Acta Metall Sin. 2019;55(5):627–37.
[49] Wei ZJ, Zhang LJ, Yang H, Shen T, Chen L. Effect of preparing method of ZnO powders on electrical arc erosion behavior of Ag/ZnO electrical contact material. J Mater Res. 2016;31(4):468–79.
[50] Xie J, Wang XH, Zhou YC. Understanding formation mechanism of titanate nanowires through hydrothermal treatment of various Ti-containing precursors in basic solutions. J Mater Sci Technol. 2012;28(6):488–94.
[51] Anjum M, Kumar R, Barakat MA. Visible light driven photocatalytic degradation of organic pollutants in wastewater and real sludge using ZnO–ZnS/Ag_2O–Ag_2S nanocomposite. J Taiwan Inst Chem Eng. 2017;77:227–35.
[52] Martina I, Wiesinger R, Jembrih-Simburger D, Schreiner M. Micro-Raman characterization of silver corrosion products. Instrumet Setup Ref Database Raman Spectrosc. 2012;9:1–8.
[53] Ravi Chandra Raju N, Jagadeesh Kumar K, Subrahmanyam A. Physical properties of silver oxide thin films by pulsed laser deposition: effect of oxygen pressure during growth. J Phys D: Appl Phys. 2009;42(13):135411.
[54] Ravi Chandra Raju N, Jagadeesh Kumar K. Photodissociation effects on pulsed laser deposited silver oxide thin films: surface-enhanced resonance Raman scattering. J Raman Spectrosc. 2011;42(7):1505–9.
[55] Jinji Y. Gas discharge. Beijng: Science Press; 1983.
[56] Beilis II. State of the theory of vacuum arcs. IEEE Trans Plasma Sci. 2001;29(5):657–70.
[57] Boddy PJ, Utsumi T. Fluctuation of arc potential caused by metal-vapor diffusion in arcs in air. J Appl Phys. 1971;42(9):3369–73.
[58] Gray EW. Some spectroscopic observations of the two regions (metallic vapor and gaseous) in break arcs. IEEE Trans Plasma Sci. 1973;1(1):30–3.
[59] Hernqvist KG. Emission mechanism of cold-cathode arcs. Phys Rev. 1958;109(3):636–46.
[60] Meunier JL, Drouet MG. Experimental study of the effect of gas pressure on arc cathode erosion and redeposition in He, Ar, and SF6 from vacuum to atmospheric pressure. IEEE Trans Plasma Sci. 1987;15(5):515–9.
[61] Drouet MG, Meunier JL. Influence of the background gas pressure on the expansion of the arc-cathode plasma. IEEE Trans Plasma Sci. 1985;13(5):285–7.
[62] Vinaricky E, Behrens V. Switching behavior of silver/graphite contact material in different atmospheres with regard to contact erosion. Proceedings of the Forty-Fourth IEEE Holm Conference on Electrical Contacts. Arlington, VA, USA; 1998. p. 292–300.
[63] Yoshida K, Takahashi A. Effects of air pressure on transition boundary from metallic to gaseous phase in W break arc. Electron Commun Jpn (Part II: Electron). 1992;75(11):71–80.
[64] Vinaricky E, Behrens V, editors. Switching behavior of silver/graphite contact material in different atmospheres with regard to contact erosion. Proceedings of the Forty-Fourth IEEE Holm Conference on Electrical Contacts; 2002.
[65] Yoshida K, Tanimoto S, editors. An experimental study of arc duration and transition from metallic to gaseous phase in Ag alloy break arc. Electrical Contacts – 2007 Proceedings of the 53rd IEEE Holm Conference on Electrical Contacts, 2007 16–19 Sept; 2007.
[66] Huang XC, Feng Y, Qian G, Liu K. Erosion behavior of Ti_3AlC_2 cathode under atmosphere air arc. J Alloy Compd. 2017;727:419–27.